



ELSEVIER

Infrared Physics & Technology 43 (2002) 335–344

INFRARED PHYSICS  
& TECHNOLOGY

www.elsevier.com/locate/infrared

# Integration of microbolometers with infrared microstrip antennas

Iulian Codreanu, Glenn D. Boreman \*

*School of Optics/CREOL, University of Central Florida, 4000 Central Florida Boulevard, P.O. Box 162700, Orlando, FL 32816-2700, USA*

Received 17 December 2001

## Abstract

We report on various integration schemes of infrared microbolometers with microstrip antennas. The first integration design consists of two gold (Au) rectangular microstrip patches coupled along the radiating edges by a narrow niobium (Nb) strip. Devices using silicon oxide are compared to devices using amorphous silicon as antenna substrate. An extension of the twin-patch detector design is the microstrip dipole antenna-coupled microbolometer. Two ways of connecting the device to the contact pads via narrow dc leads are presented and compared. The contribution of the dc leads to the detector response is eliminated by directly connecting the dipole to the contact pads. The thermal isolation of the microbolometer from the silicon wafer is improved by incorporating air into the antenna dielectric substrate. This leads to higher detector responsivity and shifts the resonance towards longer antennas. The implementation of a bridge microstrip dipole antenna structure is also discussed.

© 2002 Elsevier Science B.V. All rights reserved.

*Keywords:* IR detector; Infrared antenna; Microstrip dipole; Microbolometer

## 1. Introduction

The first antenna-coupled infrared detector was reported in 1968 and consisted of a thin, long tungsten (W) wire in contact with a metallic (silver or steel) base plate [1]. The end of the tungsten wire in contact with the metal base was sharpened using chemical etching. Because of a thin oxide layer present on the metal plate, a non-linear contact was formed between the tungsten wire and the plate. The tungsten wire acted like a long-wire

antenna for 10.6- $\mu\text{m}$  carbon dioxide ( $\text{CO}_2$ ) laser radiation. The non-linear contact rectified the electrical currents induced on the long wire.

From a practical point of view, these structures had several drawbacks. The thin, long, unsupported wires were mechanically unstable and reproducible results were very difficult to achieve. The cylindrically symmetric radiation pattern of the long wire did not allow for good antenna directivity. Also, it was impossible to arrange these “cat whiskers” in an array to form a large-area detector.

Significant improvements were achieved by using lithographic techniques. The new fabrication technique allowed for mechanically stable devices

\* Corresponding author. Tel.: +1-407-823-6815; fax: +1-407-823-6880.

E-mail address: [gboreman@mail.ucf.edu](mailto:gboreman@mail.ucf.edu) (G.D. Boreman).

and more reproducible results. It also opened the possibility of large-area detectors based on arrays. The earliest lithographic thermal IR sensors used metal–oxide–metal (MOM) diodes as detectors. MOM diodes integrated with wire-like printed antennas were reported by Small et al. [2], Wang et al. [3], and Wiesendanger and Kneubuhl [4] during the mid 1970s. The detection mechanism was based on the rectification of the terahertz (THz) currents induced on the antennas by the MOM diodes.

In the years that followed, lithographic antennas found applications mainly in the microwave and millimeter-wave spectral domains. In 1991, Grossman et al. [5] reported on an integrated sensor detecting 9.5- $\mu\text{m}$  CO<sub>2</sub> laser radiation. It consisted of a niobium microbolometer integrated with a printed gold spiral antenna. In the following years, integrated infrared detectors using lithographic dipole [6], log-periodic [7], bow-tie [8], and spiral [9] antennas were reported.

Beck and Mirotznik used the finite-difference time-domain (FDTD) method to predict the performance of microstrip patch antennas as optical couplers in quantum-well infrared detectors [10]. We report on the design, modeling, fabrication, and testing of microstrip antenna-coupled infrared microbolometers.

## 2. Device fabrication

To ensure electrical and thermal isolation of the detector from the silicon wafer, a 200-nm thick layer of silicon oxide was first deposited by plasma enhanced chemical vapor deposition (PECVD) onto the polished side of the wafer. A finite ( $30 \times 30 \mu\text{m}^2$ ) ground plane pattern was defined into a bi-layer of electron-beam resist. After evaporating 10 nm of titanium and 100 nm of gold, the excess metal was lifted off. The antenna dielectric substrate, usually consisting of silicon oxide, was deposited next. The antenna, direct current (dc) leads (where applicable) and contact pads were fabricated in one lithographic step. Nominally 100 nm of gold were electron beam evaporated on top of a patterned bi-layer of electron-beam resist. A thin (10 nm) layer of titanium was used as adhesion

layer between gold and the dielectric substrate. The excess metal was lifted off. The microbolometer was also fabricated by electron-beam lithography and lift-off. To ensure good step coverage dc magnetron sputtering was used to deposit the bolometer material.

## 3. Experimental results

The detectors were tested using 10.6- $\mu\text{m}$  wavelength, linearly polarized CO<sub>2</sub> laser radiation. The expanded and collimated laser beam was focused by  $F/1$  optics, resulting in an almost diffraction-limited spot with a  $1/e^2$  radius of 13  $\mu\text{m}$  and an irradiance of about 1000 W/cm<sup>2</sup>. The detectors under test were biased at 100 mV and placed in the focus of the laser beam. A mechanical chopper modulated the laser beam at 2.5 kHz and the change in the voltage across the terminals of the detector was recorded using a lock-in amplifier after a  $10\times$  pre-amplification.

The device was mounted on a three-axis micropositioner stage. Two computerized Melles–Griot nanomovers controlled the position of the detector in the vertical ( $x$ – $y$ ) plane. The movement along the beam-propagation direction ( $z$ ) was controlled manually. A two-dimensional (2D) scan of the detector response was recorded by moving the detector in the  $x$ – $y$  plane while the laser beam was kept fixed. The 2D response thus recorded is a convolution of the detector spatial response with the irradiance profile of the laser beam. An iterative deconvolution algorithm reported by Alda et al. [11] was used to extract the spatial response of the detector from the measured 2D scan.

The first microstrip antenna-coupled infrared detector that we investigated consisted of two gold microstrip patches connected along the radiating edges by a narrow strip of niobium acting as a bolometer. Direct coupling along the radiating edges had been previously employed to increase the impedance bandwidth of a microstrip patch antenna [12]. Fig. 1(a) shows an electron micrograph of the twin microstrip patch integrated detector. The microstrip patches were 3- $\mu\text{m}$  wide and were separated by a 370-nm gap. The patch width is measured along the horizontal ( $x$ ) direction

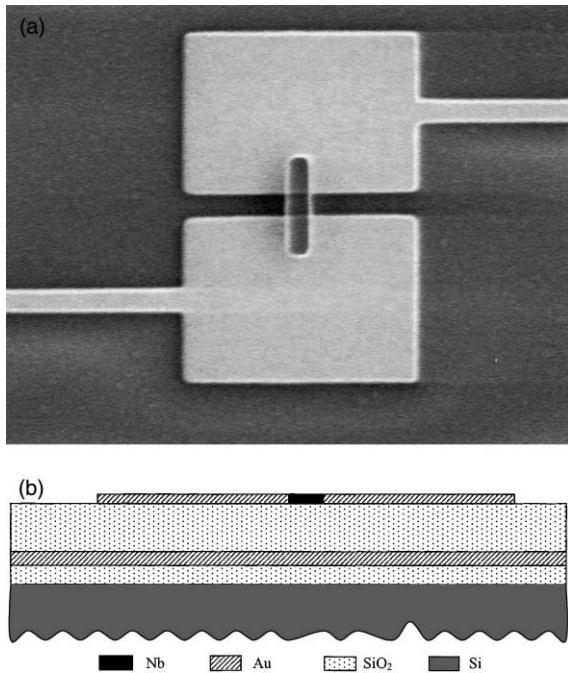


Fig. 1. Twin microstrip patch antenna-coupled microbolometer: (a) top view (electron micrograph); (b) schematic side view.

while the patch length along the vertical ( $y$ ) direction in Fig. 1(a). The 70-nm thick Nb microbolometer was 360-nm wide and 1.6- $\mu\text{m}$  long. The 400-nm wide, 100-nm thick horizontal lines (referred to as dc leads) connect the device to the contact pads. To connect the device to the biasing and read-out circuit aluminum wires were ultrasonically bonded to the contact pads. The antenna and the microbolometer were separated from the finite ground plane by a 200-nm thick layer of silicon oxide. A schematic side view of the integrated detector is shown in Fig. 1(b). The electrical resistance of the twin-patch devices was 205  $\Omega$ .

The maximum detector response was obtained when the incident radiation was normally incident on the plane of the detector and polarized along the microbolometer; cross-polarization ratios of about 20 were measured. The measured time constant of the devices was 150 ns. Detectors with five different patch lengths were fabricated and tested. Fig. 2 shows the detector response versus patch length. About 35 mW of  $\text{CO}_2$  laser radiation polarized along the bolometer were incident on

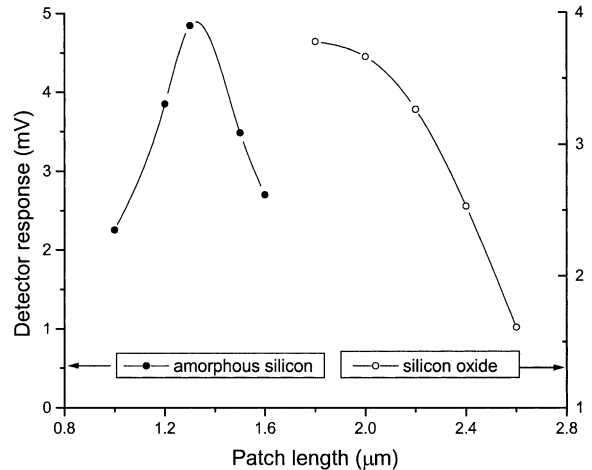


Fig. 2. Detector response versus patch length. Devices fabricated on amorphous silicon are more sensitive to changes in patch length.

the integrated sensor. Also shown is the response given by twin microstrip patch antenna-coupled microbolometers separated from the ground plane by a 250-nm thick layer of amorphous silicon. Those microstrip patches were 2.0- $\mu\text{m}$  wide and the electrical resistance of the integrated detectors was about 300  $\Omega$ . The maximum detector response occurred at shorter patches because amorphous silicon has a higher dielectric constant (11.7) compared to silicon oxide (4.0). The detectors fabricated on amorphous silicon are more sensitive in changes in the patch length because of the higher dielectric constant.

A typical detector response versus the wavelength of the incident radiation is shown in Fig. 3 for a device with a patch length of 2  $\mu\text{m}$  fabricated on a 200-nm thick layer of silicon oxide backed by a gold ground plane. Fig. 4 shows the resonant wavelength versus patch length for devices using silicon oxide as substrate and for devices using amorphous silicon as substrate. The resonant wavelength of devices using amorphous silicon as antenna substrate is more sensitive to changes in patch length than the devices using silicon oxide as antenna substrate because the bandwidth of a microstrip antenna is inversely proportional to the square root of the dielectric constant of the substrate [12].

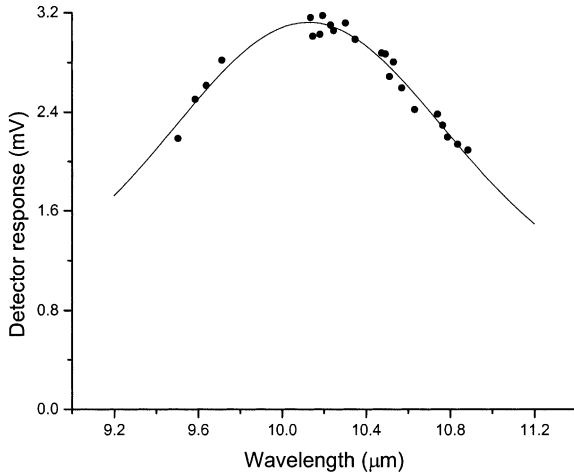


Fig. 3. Detector response versus the wavelength of the incident radiation. The continuous line curve represents a Gaussian fit of the experimental data.

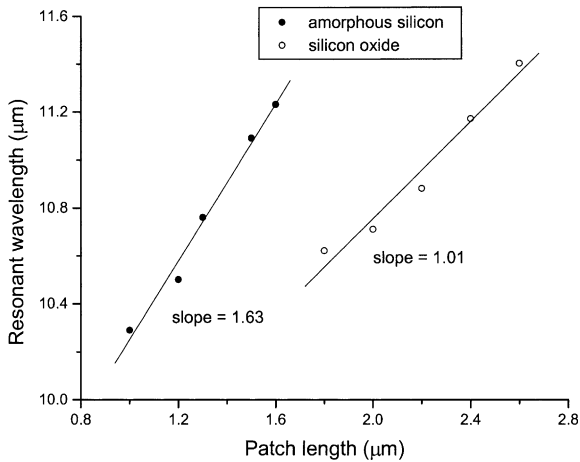


Fig. 4. Device resonant wavelength versus patch length.

Fig. 5 compares the *E*- and *H*-plane radiation patterns for a twin microstrip patch antenna fabricated on silicon oxide with a 1.8- $\mu\text{m}$  long patch. The incident radiation was polarized along the microbolometer. The *E*-plane is perpendicular to the plane of Fig. 1(a) and intersects the bolometer along its length (*y*-direction). The *H*-plane contains the normal to the plane of the figure and is perpendicular to the *E*-plane. To record the radiation patterns the detector plane was rotated while the laser beam was maintained fixed. The maximum detector response was obtained when the

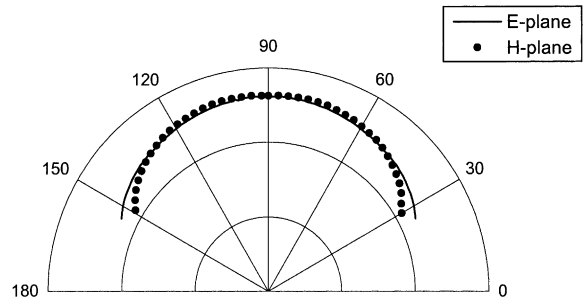


Fig. 5. Detector response versus angle of incidence. Both the *E*- and *H*-plane are broadside.

laser beam was normally incident on the plane of the detector, i.e. the radiation pattern is broadside. At near-grazing incidence the *H*-plane response drops faster than the *E*-plane response. A similar behavior is observed for a single rectangular microstrip patch antenna [13].

The impedance of a microstrip line is very sensitive to its width [13]. To improve the impedance matching between the antenna and its load the width of the Nb microbolometer was set equal to the width of the microstrip patches leading to a *microstrip dipole* antenna-coupled IR detector (Fig. 6). The side view of the device was similar to Fig. 1(b). The two antenna arms were nominally 1.8- $\mu\text{m}$  wide and were separated by a 400-nm gap. The electron micrograph shown in Fig. 6 was taken before the Nb microbolometer was deposited. A rectangular ( $1.8 \times 1.0 \mu\text{m}^2$ ) bolometer pattern,

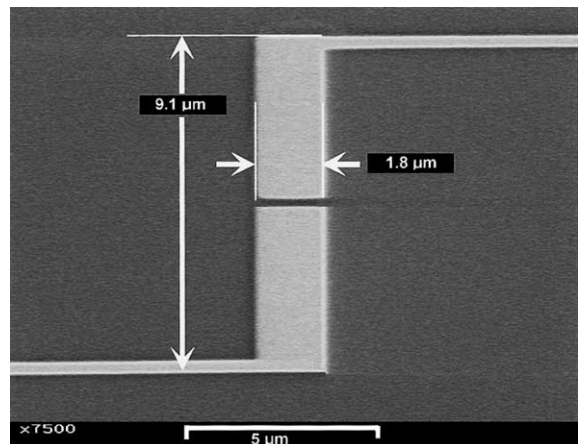


Fig. 6. Microstrip dipole antenna with dc lines connected at the ends of the dipole.

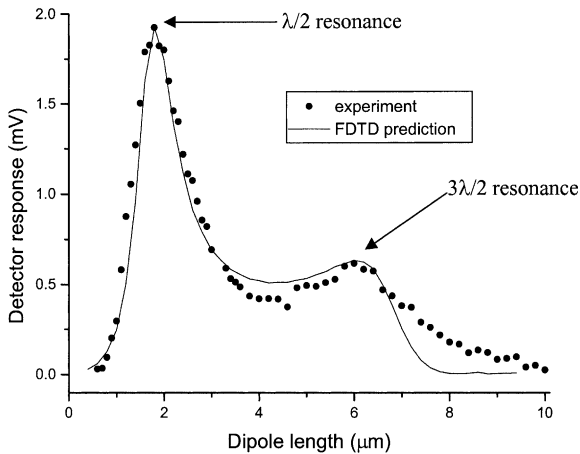


Fig. 7. Measured detector response for versus dipole length along with the predicted detector response.

defined in an electron-beam resist layer, was aligned with the gap between the two antenna arms. A 100-nm thick layer of Nb was deposited by dc magnetron sputtering and the excess metal was lifted off. The antenna was separated from the ground plane by a 500-nm thick layer of silicon oxide. The dc electrical resistance of the detectors was about 45  $\Omega$ .

Antennas with full lengths ranging from 0.6 to 10.6  $\mu\text{m}$  were fabricated in 0.1- $\mu\text{m}$  increments. Fig. 7 shows the measured detector response versus antenna length along with the detector response predicted by the FDTD method. The incident  $\text{CO}_2$  laser radiation was polarized along the antenna arms. The half-wave resonance occurs for a 1.8- $\mu\text{m}$  long microstrip dipole antenna. The first minimum in the detector response, appearing around 4.2  $\mu\text{m}$ , corresponds to a full-wave antenna. The 3/2-wave resonance occurs for a 6.0- $\mu\text{m}$  long antenna. Fig. 8 shows the response of a detector whose antenna was 1.6- $\mu\text{m}$  long as a function of the wavelength of the incident radiation together with the FDTD predicted response.

The spatial response of a microbolometer integrated with two antennas of different lengths is shown in Fig. 9. A schematic top view of the integrated detector is superimposed onto the spatial response. The contour lines represent 10% increments of the maximum detector response. The response is elongated along the horizontal direc-

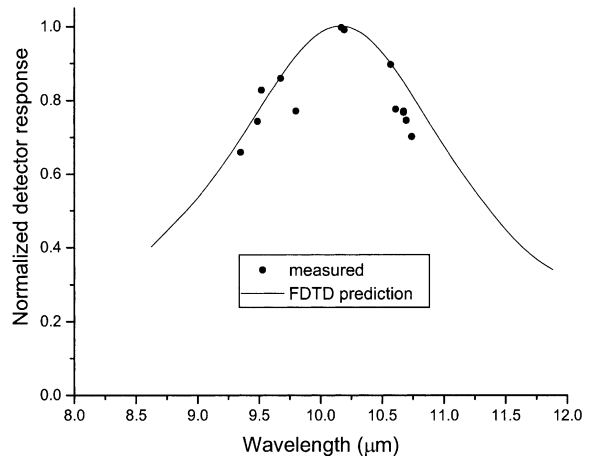


Fig. 8. Detector response versus wavelength of the incident radiation. The microbolometer was integrated with a 1.6- $\mu\text{m}$  long microstrip dipole.

tion because of the dc leads. They collect infrared radiation and also provide a low-thermal-impedance conduction path for the heat generated within the oxide substrate to reach the microbolometer. The antenna length of the device whose spatial response is shown in Fig. 9(a) is close to the resonant length (see Fig. 7) and therefore the antenna response is strong. An increase in the antenna length leads to a larger separation between the dc leads. The dc leads have a stronger influence on the spatial response of the device with a longer antenna because the antenna response is comparable to the dc leads response. Therefore, the contribution of the dc leads to the overall detector response depends on the antenna length.

To make the separation between the horizontal dc leads independent of the antenna length, a slightly modified microstrip dipole antenna design was implemented (Fig. 10). The integrated detector had the same dimensions and the same constitutive layers as the detector shown in Fig. 6. Fig. 11 compares the detector response versus antenna length for devices with constant dc leads separation and for devices with variable distance between the dc leads. The detectors were illuminated with 10.6- $\mu\text{m}$  wavelength  $\text{CO}_2$  laser radiation. For long antennas, the devices with constant separation between the dc leads are better matched to the FDTD prediction.

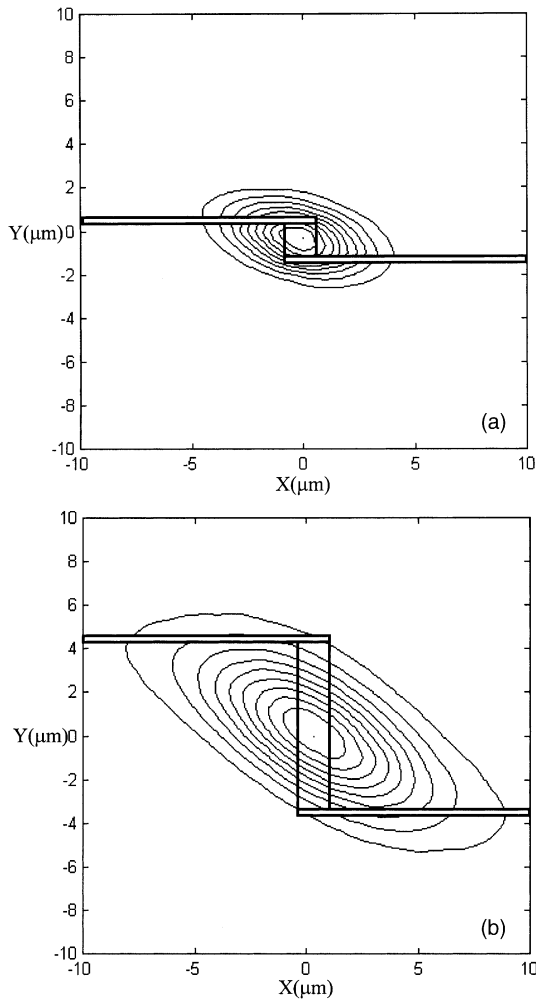


Fig. 9. Spatial response for devices with variable distance between the dc leads: (a)  $L = 1.8 \mu\text{m}$ ; (b)  $L = 8.6 \mu\text{m}$ . The contour lines represent 10% increments of the maximum detector response.

The time constant of the microstrip dipole antenna-coupled microbolometers separated from the ground plane by a 500-nm thick layer of silicon oxide was 390 ns. To increase the thermal isolation between the microbolometer and the ground plane, an air layer was incorporated into the antenna substrate. After the finite ground plane was defined, a 120-nm thick layer of oxide was deposited by PECVD at 275 °C. A 220-nm thick negative resist (NEB-31) was then spun on top of

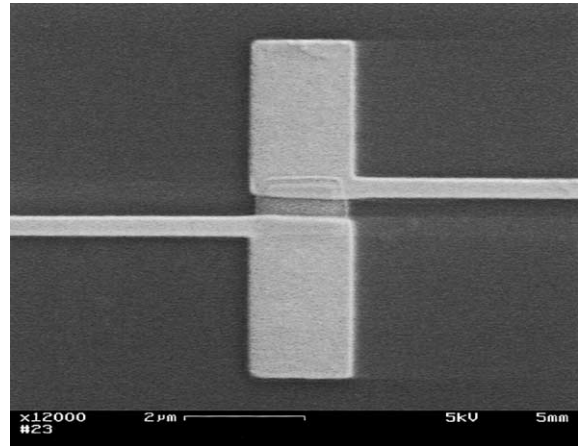


Fig. 10. Microstrip dipole antenna with fixed separation between the dc leads.

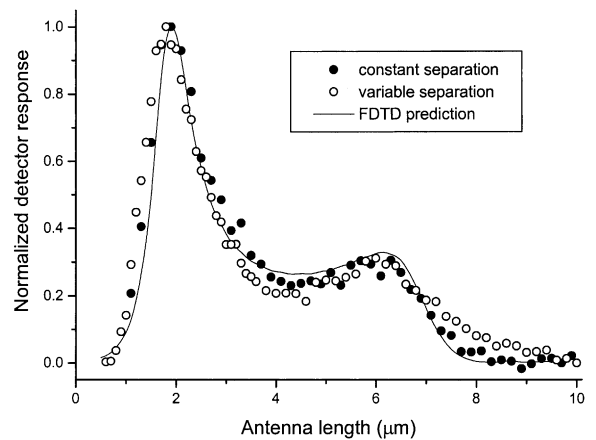


Fig. 11. Detector response for 10.6- $\mu\text{m}$   $\text{CO}_2$  radiation versus dipole length. Devices with fixed dc leads separation are better matched to the FDTD predicted detector response.

the oxide layer and patterned by electron-beam lithography. A second layer of oxide (160-nm thick) was deposited by PECVD at 150 °C on top of the patterned NEB. After the fabrication of the antenna and the microbolometer, windows were opened into the top oxide layer by reactive ion etching. The resist between the two oxide layers was removed with oxygen plasma in a barrel etcher. Fig. 12(a) shows an electron micrograph of the device after the NEB layer was etched with the

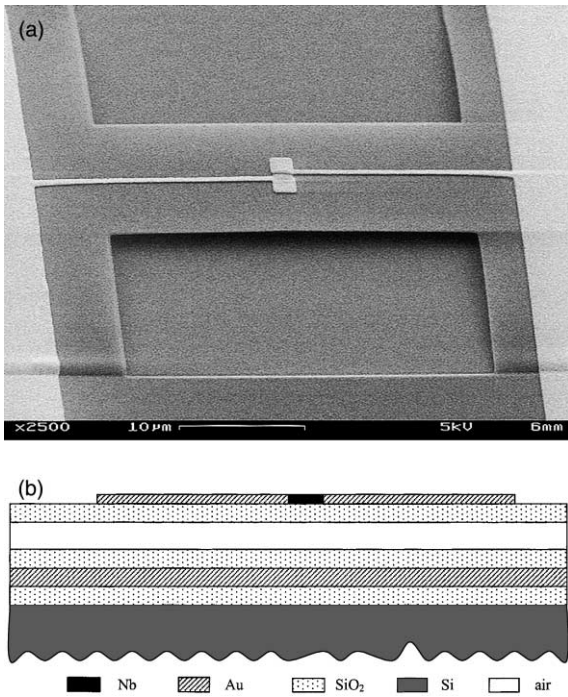


Fig. 12. Microstrip dipole antenna incorporating an air layer within the dielectric substrate: (a) electron micrograph; (b) side view schematic.

oxygen plasma. The top oxide layer provides physical support for the antenna and the dc leads. A schematic side view of the device is shown in Fig. 12(b).

Fig. 13 compares the normalized detector response versus antenna length for devices separated from the ground by a continuous layer of oxide and devices incorporating an air layer into the dielectric spacer. The distance between the antenna and the ground was nominally 500 nm for both types of detectors. The continuous line curves represent the predicted detector response by FDTD method. The locations of the antenna resonances shift toward longer dipoles when the air layer is sandwiched between the oxide layers. At the same time, the bandwidth of the first resonance is widened because the effective dielectric constant of the dielectric spacer is reduced. Because of better thermal isolation the responsivity of the devices incorporating the air layer within their substrate is 45 times larger than the responsivity of

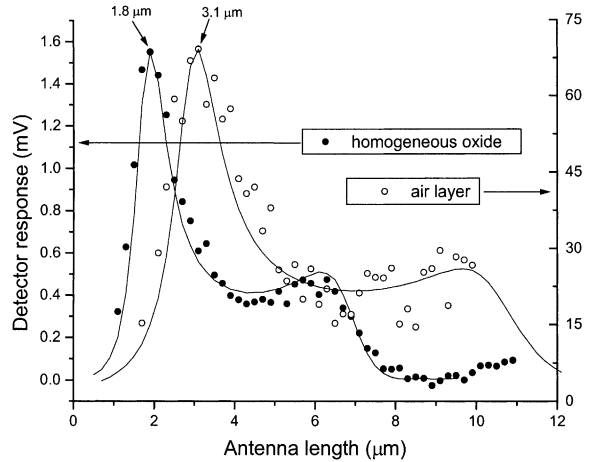


Fig. 13. Detector response versus dipole length. The air layer shifts the resonance towards longer antennas. The continuous line curves represent the FDTD predicted detector response.

the devices with oxide substrate. Correspondingly, the devices with the sandwiched substrate are 45 times slower than the devices with homogeneous oxide substrate.

To eliminate the contribution of the dc leads to the detector response the dipole antenna was directly connected to the contact pads (Fig. 14). The constitutive thin-film layers are shown in Fig. 1(b). The 350-nm wide, 100-nm thick antenna arms

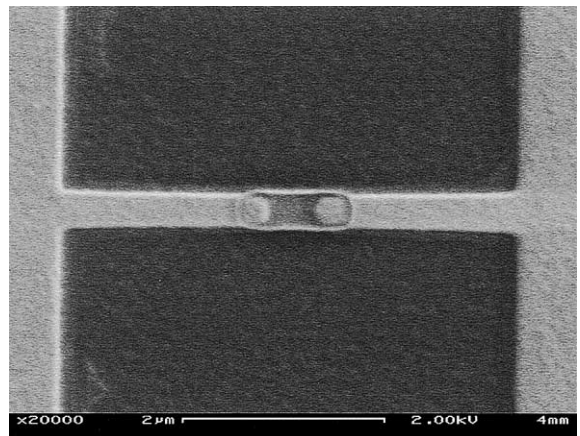


Fig. 14. Microstrip dipole directly connected to the contact pads.

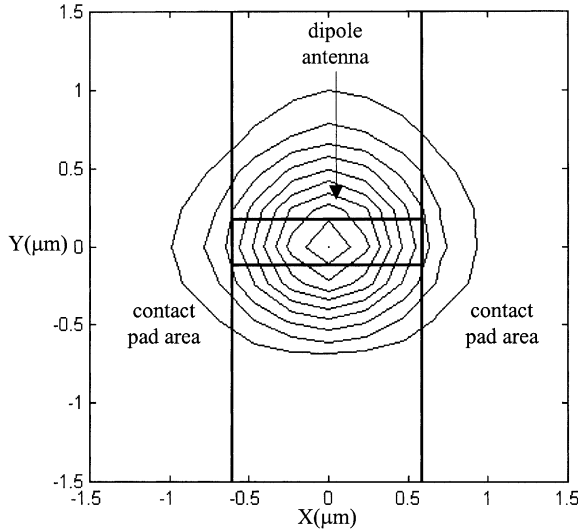


Fig. 15. Deconvolved spatial response of a 1.2- $\mu\text{m}$  long microstrip dipole antenna directly connected to the contact pads. The contours represent 10% increments of the maximum detector response.

were separated by a 1- $\mu\text{m}$  long gap. The niobium microbolometer was 1.8- $\mu\text{m}$  long, 400-nm wide and 100-nm thick. A 500-nm thick layer of silicon oxide separated the antenna from the ground plane.

The detector spatial response shown in Fig. 15, corresponding to a 1.2- $\mu\text{m}$  long dipole directly connected to the contact pads, is almost entirely confined between the contact pads. Fig. 16 compares the normalized detector response for devices connected via dc leads and for devices connected directly to the contact pads. Both sets of devices give maximum response for a 1.8- $\mu\text{m}$  long antenna. However the response of the devices connected directly to the contact pads is less sensitive to changes in antenna length. This could be attributed to the fact that the dipoles connected directly to the contact pads are not open ended; the electrical currents induced along the dipole are partially transmitted into the contact pads. Thus, the effective *electrical length* of the dipole connected directly to the contact pads is not as precisely defined as for antennas with dc leads, especially for small separations between the contact pads.

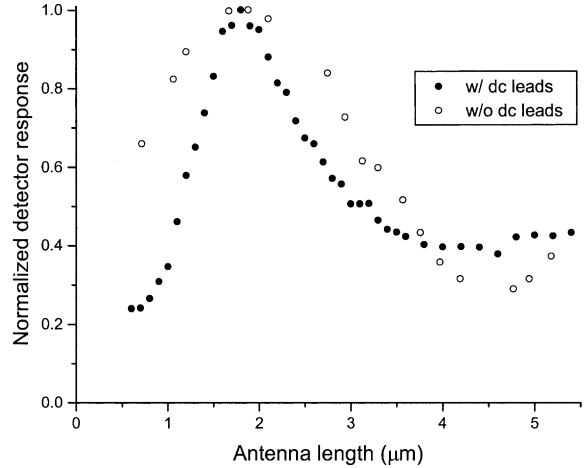


Fig. 16. Detector response to 10.6- $\mu\text{m}$   $\text{CO}_2$  radiation versus dipole length. Devices with dc leads are more sensitive to changes in antenna length.

The fabrication of devices with sub-micron separation between the contact pads was difficult because of the lithographic proximity effect. To shift the resonance towards longer dipoles, eliminate the absorption in the dielectric layer, and improve the thermal isolation between the microbolometer and the ground plane, we eliminated the silicon oxide between the antenna and the ground plane. Fig. 17(a) shows a microstrip dipole antenna suspended above the ground plane. A schematic of the thin-film layers making up the integrated detector is shown in Fig. 17(b). A 500-nm thick layer of NEB-31 was spun on top of the finite ( $30 \times 30 \mu\text{m}^2$ ) ground plane. The resist layer was patterned into a square ( $40 \times 40 \mu\text{m}^2$ ) post-aligned with the finite ground. A rectangular ( $1.0 \times 2.0 \mu\text{m}^2$ ) microbolometer pattern was defined into a bi-layer of e-beam resist spun on top of the NEB layer. A 40-nm thick layer of titanium was e-beam evaporated and the excess metal was lifted off. The antenna and the contact pads pattern, defined into a bi-layer of e-beam resist, was aligned with the titanium microbolometer. After the evaporation and lift-off of the antenna metal (200-nm thick layer of gold), an oxygen plasma isotropic etch was used to remove the NEB from under the bridge dipole.

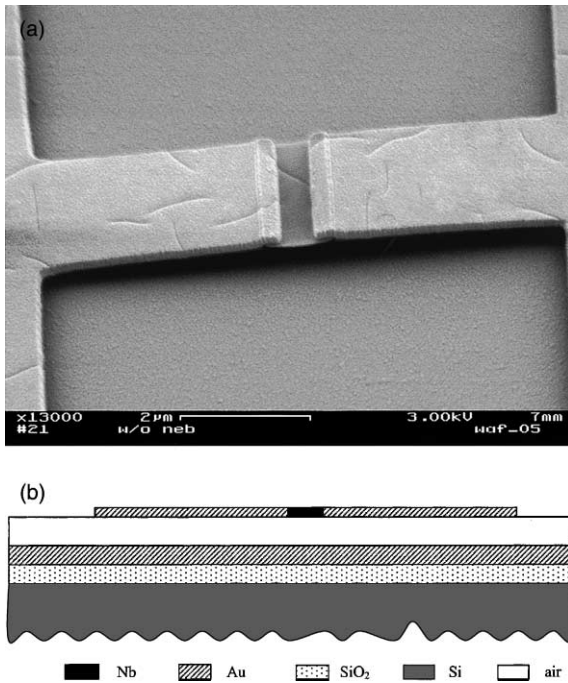


Fig. 17. Bridge microstrip dipole antenna-coupled microbolometer: (a) electron micrograph; (b) side view schematic.

The measured detector response versus antenna length is shown in Fig. 18 along with the FDTD prediction. Removing the oxide between the an-

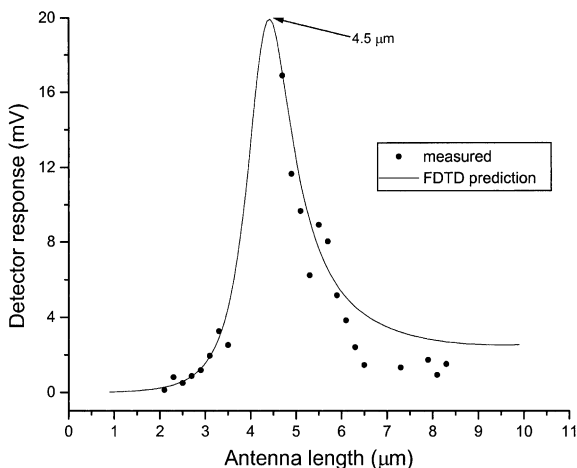


Fig. 18. Detector response to 10.6- $\mu\text{m}$   $\text{CO}_2$  radiation versus bridge dipole length.

tenna and the ground plane shifts the resonance to a 4.5- $\mu\text{m}$  antenna length. By shifting the resonance to longer antennas the bridge dipole design relaxes the lithographic requirements. This opens the possibility of using step-and-repeat optical lithography techniques for the fabrication of antenna-coupled infrared detectors. The fabrication throughput can be considerably increased by using optical lithography, especially for antenna-coupled focal plane arrays.

#### 4. Conclusions

We studied the integration of metallic microbolometers with gold microstrip antennas for the detection of mid-infrared radiation. Two rectangular microstrip patches were directly coupled along the radiating edges by a narrow niobium bridge. Devices with five patch lengths were fabricated on a silicon oxide substrate. The detector response to 10.6- $\mu\text{m}$   $\text{CO}_2$  laser radiation was sensitive to the length of the microstrip patch. The detector response was polarized along the microbolometer. The  $E$ - and  $H$ -plane radiation patterns were broadside. Devices fabricated on amorphous silicon resonated at shorter patch lengths because of the higher dielectric constant. The response of the detectors versus the wavelength of the incident radiation confirmed that devices fabricated on amorphous silicon have a narrower bandwidth.

The logical extension of the twin microstrip patch detector was the microstrip dipole antenna-coupled microbolometer. In a first design, the dc leads were placed at the ends of the dipole. Detectors with dipole lengths ranging from 0.6 to 10.6  $\mu\text{m}$  were fabricated and tested. The study of the detector response to 10.6- $\mu\text{m}$   $\text{CO}_2$  radiation versus dipole length allowed us to identify the first three dipole resonances. The experimental data agreed well with numerical predictions based on the FDTD method. Connecting the dc leads at the end of the dipole makes the separation between the leads dependent on the dipole length. The amount of coupling between the dc leads depends on the separation between them. Both by collecting IR radiation, and by providing a thermal conduction

path for the heat generated within the antenna substrate to the microbolometer, the dc leads contribute to the detector response. To keep the contribution of the dc leads independent of the dipole length, a design with fixed separation between the dc leads was implemented. The agreement between the FDTD predictions and the experimental data for the new design is excellent, even for long dipoles.

To improve the detector responsivity and to shift the resonance towards longer antennas a layer of air was incorporated into the microstrip dipole dielectric substrate. Compared to detectors with homogeneous dielectric spacer of similar thickness, both the detector responsivity and the time constant increased by a factor of 45. The antenna resonance shifted to longer antenna lengths and the bandwidth of the resonance increased because of the lower effective dielectric constant.

The contribution of the dc leads to the detector response was eliminated by connecting the dipole directly to the contact pads. However, this makes the fabrication process more difficult for short dipoles because of lithographic proximity effects. Moreover, the detector response is less sensitive to changes in antenna length because the electrical length of the dipoles is not precisely defined since the induced antenna currents are partially transmitted into the contact pads.

To relax the lithographic requirements, to reduce the amount of IR radiation absorbed into the dielectric substrate, and to improve the thermal insulation of the microbolometer from the ground plane, a bridge microstrip dipole-coupled microbolometer was successfully implemented. The resonance of the microstrip dipole was shifted to a 4.5- $\mu\text{m}$  long antenna in the bridge configuration. The lithographic fabrication requirements are relaxed for the bridge microstrip dipole. This opens the possibility of high-throughput step-and-repeat optical lithographic fabrication techniques.

## Acknowledgements

This material is based upon work supported by NASA under grant no. NAG5-10308.

## References

- [1] L.O. Hocker, D.R. Sokoloff, V. Daneu, A. Szoke, A. Javan, Frequency mixing in the infrared and far-infrared using a metal-to-metal point contact diode, *Appl. Phys. Lett.* 12 (12) (1968) 401–402.
- [2] J.G. Small, G.M. Elchinger, A. Javan, A. Sanchez, F.J. Bachner, D.L. Smythe, Ac electron tunneling at infrared frequencies: thin-film M–O–M diode structure with broad-band characteristics, *Appl. Phys. Lett.* 24 (1974) 275–279.
- [3] S.Y. Wang, T. Izawa, T.K. Gustafson, Coupling characteristics of thin-film metal–oxide–metal diodes at 10.6  $\mu\text{m}$ , *Appl. Phys. Lett.* 27 (9) (1975) 275–279.
- [4] E. Wiesendanger, F. Kneubuhl, Thin-film MOM-diodes for infrared detection, *Appl. Phys.* 13 (1977) 343–349.
- [5] E.N. Grossman, J.E. Sauvegeau, D.G. McDonald, Lithographic spiral antennas at short wavelengths, *Appl. Phys. Lett.* 59 (25) (1991) 3225–3227.
- [6] I. Wilke, W. Hermann, F.K. Kneubuhl, Integrated nanostrip dipole antennas for coherent 30 THz infrared radiation, *Appl. Phys. B* 58 (1994) 87–95.
- [7] N. Chong, H. Ahmed, Antenna-coupled polycrystalline silicon air-bridge thermal detector for mid-infrared radiation, *Appl. Phys. Lett.* 71 (12) (1997) 1607–1609.
- [8] C. Fumeaux, W. Hermann, H. Rothuizen, P. De Natale, F.K. Kneubuhl, Mixing of 30 THz laser radiation with nanometer thin-film Ni–NiO–Ni diodes and integrated bow-tie antennas, *Appl. Phys. B* 62 (1996) 135–140.
- [9] C. Fumeaux, G.D. Boreman, W. Hermann, H. Rothuizen, P. De Natale, F.K. Kneubuhl, Polarization response of asymmetric spiral infrared antennas, *Appl. Opt.* 36 (25) (1997) 6485–6490.
- [10] W.A. Beck, M.S. Mirotznik, Microstrip antenna coupling for quantum-well infrared photodetectors, *Infrared Phys. Technol.* 42 (2001) 189–198.
- [11] J. Alda, C. Fumeaux, I. Codreanu, J.A. Schaefer, G.D. Boreman, Deconvolution method for two-dimensional spatial-response mapping of lithographic infrared antennas, *Appl. Opt.* 38 (19) (1999) 3992–4000.
- [12] G. Kumar, K.C. Gupta, Directly coupled multiple resonator wide-band microstrip antennas, *IEEE Trans. Antennas Propagat.* 33 (60) (1985) 588–593.
- [13] C.A. Balanis, *Antenna theory: analysis and design*, John Wiley & Sons, New York, 1997.